

A Numerical Study of Chaotic Dynamics in Thermal Ignition and Chemically Reactive Swirling Flow

W. E. Tavernetti*, M. M. Hafez*
Corresponding author: etavernetti@math.ucdavis.edu

* University of California Davis, USA.

Abstract: Nonlinear dynamical phenomena in combustion processes is an active area of experimental and theoretical research. This is in large part due to increasingly strict environmental pressures to make gas turbine engines and industrial burners more efficient. Using numerical methods, this study examines chaotic dynamics in a thermal ignition framework as well as axisymmetric swirling flow leading to enhanced mixing with vortex breakdown. The incompressible and compressible, reactive Navier-Stokes equations in terms of stream function, vorticity, circulation are used. Results, details of the numerical algorithms, as well as numerical verification techniques and validation with sources from the literature will be presented. Understanding how instabilities are affected by modeling reactant consumption are the main goals of this study.

Keywords: Combustion, Ignition, Vortex Breakdown, Chaos.

1 Introduction

Combustion is an interdisciplinary field combining elements from fluid dynamics, chemical kinetics and transport phenomena. The general problem is governed by the reactive, time dependent, compressible Navier–Stokes equations for several chemical species. Difficulties that will be addressed are multiple time scales, non-linearity (both in the advection and chemical source terms) and combustion instabilities in transitions to unsteady oscillatory and aperiodic solutions. The fluid mechanics foundation is the compressible Navier–Stokes equations. The chemical kinetics foundations are dynamics and chemical process rate governing laws, such as the Arrhenius law. The transport phenomena foundations are momentum dissipation, heat conduction and mass diffusion. A continuum approximation is assumed for the density, pressure, velocity, and temperature by requiring these quantities are at least weakly differentiable. In the reactive case, in contrast to the cold case, where it is sometimes a good approximation, the flow cannot be assumed isothermal, or isentropic (where shocks are present in transonic flow or choked nozzle flows). Conservation of mass, momentum, energy and the perfect gas law, $P = \rho RT$, must be satisfied. The non-dimensional reactive, time dependent, compressible Navier–Stokes equations in non-conservative form for $i = 1, \dots, N$ chemical species

[†] This material is based upon work supported by the National Science Foundation under DMS-0636297.

^λ The second author likes to acknowledge the summer support of NASA Ames (grant # NNX09AM34A).

are given by Kuo, [17]:

$$\begin{aligned}
 \frac{\partial \rho}{\partial t} + \nabla \cdot (\rho V) &= 0 \\
 \rho \frac{\partial V}{\partial t} + \rho V \cdot \nabla V &= -\nabla p + \frac{1}{Re} [\nabla \cdot \tau_{ij}] + f \\
 \rho \frac{\partial Y_i}{\partial t} + \rho V \cdot \nabla Y_i &= \frac{1}{Sc \cdot Re} \nabla^2 Y_i - \Omega_i \\
 \rho \frac{\partial H}{\partial t} + \rho V \cdot \nabla H &= \frac{\partial p}{\partial t} + \frac{1}{Pr \cdot Re} \nabla^2 T + \nabla \cdot (V \cdot \tau_{i,j}) \\
 p &= \rho T \frac{\gamma - 1}{\gamma}
 \end{aligned} \tag{1}$$

Where V is the velocity vector, p, ρ, H, Y_i are the scalar pressure, density, total enthalpy and chemical species functions respectively. Body forces, such as gravity, are denoted by f . Here, the total enthalpy, H , is given in the energy equation as:

$$H = \sum_i h_i Y_i, \quad h_i = \int_{T_0}^T C_p d\tilde{T} + h_i^0 \tag{2}$$

and $\tau_{i,j}$ is given by:

$$\tau_{i,j} = \lambda \frac{\delta u_k}{\delta x_k} \delta_{i,j} + \mu \left(\frac{\delta u_i}{\delta x_j} + \frac{\delta u_j}{\delta x_i} \right), \quad \lambda = \frac{2}{3} \mu \tag{3}$$

γ is the specific heat ratio. Pr, Re, Sc are all dimensionless parameters. $Pr = \frac{\mu C_p}{k}$ is the Prandtl number which is defined as the ratio of viscous dissipation rate over thermal diffusion rate, where k is the thermal conductivity, μ is the dynamic viscosity, and C_p is the specific heat. $Re = \frac{\rho V L}{\mu}$ is the Reynolds number which is defined as the ratio of inertial over viscous stress. $Sc = \frac{\mu}{\rho D_m}$ is the Schmidt number which is defined as the ratio of the viscous dissipation rate over the mass diffusion rate. To define Ω_i , which is given by the rate of production of the species Y_i , consider the chemistry governed by an arbitrary non-elementary reversible R-reactions in N-species, where for $r = 1, \dots, R$ and stoichiometric coefficients ν :



We consider the case of an irreversible reaction law: *reagents* \rightarrow *products*. By the law of mass action, the rate chemical species are produced is proportional to the product of the concentrations of reacting species raised to their respective stoichiometric coefficient ν . The reaction specific rate of production is given by the reaction rate times the reagent-product stoichiometric balance, where for each reaction $C_i \in [0, 1]$ is the concentration of species Y_i . One elementary approach to include the physical effect of chemical kinetics is to assume a one-step reaction model. This idea can be further reduced to a premixed model, which consists of a single fuel species reacting to form products. The chemical coupling is governed by an Arrhenius heat release law. The chemistry obeys Arrhenius kinetics when the chemical rate and temperature forcing functions are of the form: $D_a \exp(-\theta/T)$. This proportionality between reaction rate and temperature is chosen specifically because it is experimentally validated. There are tuning parameters: the pre-exponential collision frequency factor D_a and θ which is proportional to the activation energy. D_a is called the Dahmkoler number which is typically the ratio of the characteristic fluid time over the characteristic chemical reaction time:

$$K := D_a T^\alpha e^{-\frac{\theta}{T}} \tag{5}$$

where $\theta = \frac{E_a}{R_{gas}}$. These quantities are determined experimentally in applications. For an ideal gas:

$$C_i = \left(\frac{p_i}{R_u T} \right) = \frac{\rho_i}{W_i} = \frac{Y_i \rho}{W_i} \tag{6}$$

where R_u is the universal gas constant, p_i is the partial pressure of the i -th species, ρ_i, ρ are densities for each species and the fluid mixture respectively, and W_i is the molecular weight of the i -th species. From this and the definitions:

$$\Omega_i = \rho \frac{\partial Y_i}{\partial t} = W_i \frac{\partial C_i}{\partial t} \quad (7)$$

it follows that species production term in the governing equations is:

$$\Omega_i = W_i \sum_{r=1}^R \left[K_r^f (\nu_{ri}'' - \nu_{ri}') \rho^{m_f} \prod_{i=1}^N \left(\frac{Y_i}{W_i} \right)^{\nu_{ri}'} - K_r^b (\nu_{ri}'' - \nu_{ri}') \rho^{m_b} \prod_{i=1}^N \left(\frac{Y_i}{W_i} \right)^{\nu_{ri}''} \right] \quad (8)$$

where $m_f = \sum_{i=1}^N \nu_i'$ and $m_b = \sum_{i=1}^N \nu_i''$. The case of a single fuel species reacting in one-step with an excess of oxidizer in an elementary irreversible reaction is a special case of the form:



This approach can be used in place of detailed chemical kinetics to emphasize the effect of heat release on the flow [?]. In this case the reaction is one-step ($R = 1$) irreversible ($K^b = 0$) involving a single premixed fuel ($N = 2$) and an excess of oxidizer ($\nu_{fuel} = 1$) with constant pre-exponential frequency factor ($\alpha = 0$):

$$\Omega = D_a \rho e^{-\theta/T} Y \quad (10)$$

where $Y = Y_{fuel}$ and for $W = 1$ for simplicity. Increasing temperature increases the reaction rate, potentially extremely slowly, until a critical temperature range is reached and then the Arrhenius function explodes approaching unity very rapidly by comparison. The Arrhenius rate law contributes not only to the stiffness of the problem, but also to the interesting structure of the solution space.

2 Thermal Ignition Theory

The goals of this study are to (1) to treat the thermal ignition problems, (2) consider the issues related to bifurcations and chaotic dynamics, and (3) implement a robust numerical method for these stiff, nonlinear, problems.

2.1 Unsteady and Steady Thermal Ignition Theory

One important starting point is simply freezing the fluid mechanics and studying chemical coupling. However, historically the problem was reduced further to an energy equation for temperature. If the chemistry is frozen, this produces the simplest possible case of the combustion problem: a 1D, viscous, constant pressure, reaction diffusion equation, or semilinear heat equation, known as the Frank-Kamenetskii solid fuel ignition model for a temperature $T(r, t)$:

$$c\sigma T_t = \kappa \nabla_r^2 T + Q\sigma A e^{-\frac{E}{RT}} \quad (11)$$

where: $\nabla_r^2 = \frac{\partial^2}{\partial r^2} + \frac{n-1}{r} \frac{\partial}{\partial r}$ with $n = 1, 2, 3$ depending on the geometry (slab, cylinder and sphere respectively) [16]. The exponential temperature source term is known as an Arrhenius law, which relates equilibrium rate constants to heat of reaction. Typical initial and boundary conditions are:

$$T = T_0 \text{ for } r = a_0 \in \mathbb{R}, \quad \frac{\partial T}{\partial r} = 0 \text{ at } r = 0, \text{ and, } T = T_0 \text{ at } t = 0 \quad (12)$$

Through a non-dimensionalization this equation can be rewritten as:

$$\theta_t = \nabla_r^2 \theta + \delta e^{\frac{\theta}{1+\epsilon\theta}} \quad (13)$$

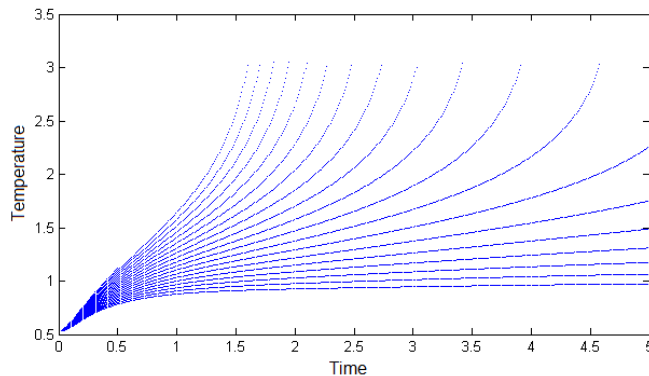


Figure 1: $\theta(r = 0.18)$, for dimension $n = 1$, unsteady solutions for a range of δ values.

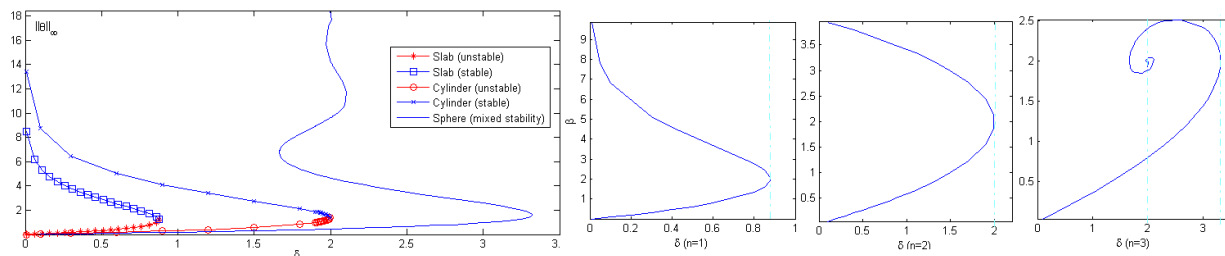


Figure 2: $\|u(r)\|_\infty$ vs. δ steady state loci (left) and the $\delta - \beta$ curves (right)

This equation, which is a perturbed Gelfand equation, is sometimes called the *small losses solid fuel ignition model* [1]. Note that $t = \tau, r = \bar{r}$ have been non-dimensionalized as well, but for convenience we them as r and t . In this form $\theta(\bar{r}, \tau)$ gives the temperature excess and $\epsilon = \frac{R\theta_{ambient}}{E}$ is the dimensionless measure of activation energy, which is typically small (i.e. about 1/50) [16]. For small ϵ , this model can be approximated as:

$$\theta_t = \nabla_r^2 \theta + \delta e^\theta \quad (14)$$

In Figure 1, for dimension $n = 1$, this problem is integrated for a range of δ values using $\theta(r_i) = \sin(\pi r_i)$ for $r \in [0, 1]$ as an initial condition, and θ at $r = 0.18$ is plotted. This result is in agreement with published results in [30]. The transition from slow reaction to explosive (or thermal runaway) behavior is shown as δ is increased. There is a critical value of δ whereby solutions above that value tend to infinity in finite time while below that they eventually approach a steady state. This δ defines the transition point between stable and unstable solution branches. The steady state theory is governed by the radially symmetric semilinear elliptic ODE and boundary conditions:

$$\begin{aligned} \nabla_r^2 \theta &= -\delta e^\theta, & r \in \Omega \\ \theta &= 0, & r \in \partial\Omega \end{aligned} \quad (15)$$

The values along the steady state loci, defined by the parameter δ , were produced using two different methods: (1) linear shooting with a 4th order Runge-Kutta solver (RK-4) and a bisection correction, and (2) a Newton residual corrector method. The loci and $\delta - \beta$ curves, where $\beta = u_r(-1)$, were produced using a parameter continuation method on δ . The results, shown in Figure 2, are in excellent quantitative agreement with published results, see for example [1], [16]. In this equation, c is the material specific heat capacity, Q is the reaction exothermicity, R is the gas constant, E is the activation energy, σ is the density, A is a rate constant, and κ is the thermal conductivity. This law defines the rate of change of temperature at spatial points in an exothermically reacting mass. In this model chemical consumption of reactants is neglected. The key results concern dynamical issues related to geometry dependent bifurcations in the solution space.

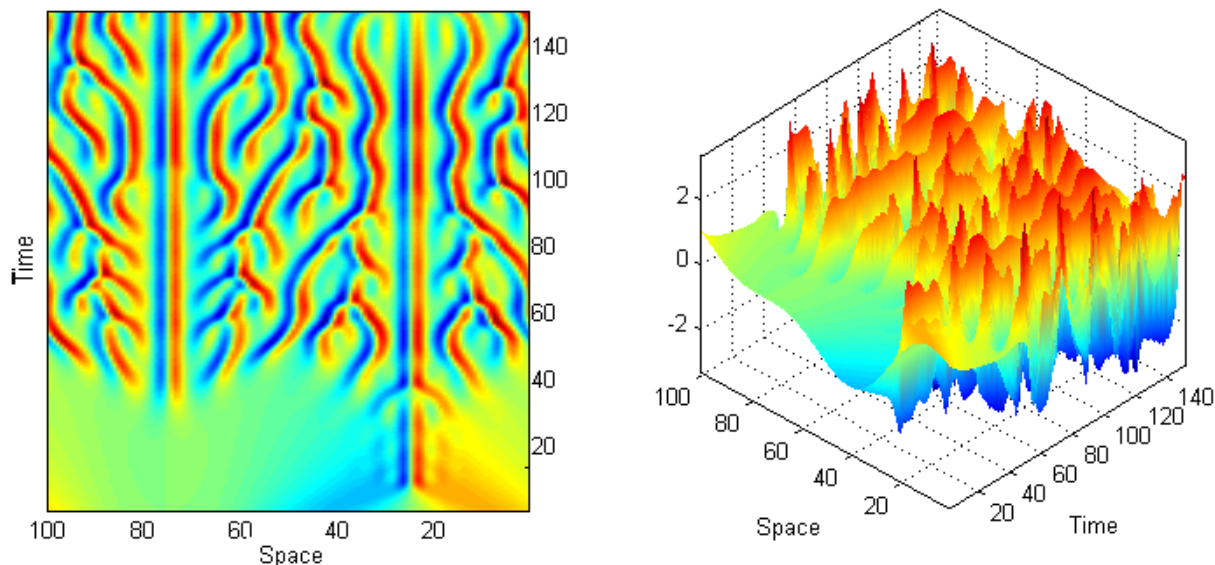


Figure 3: 1D Kuramoto-Sivashinsky chaotic solution.

The behavior of these problems can somewhat surprisingly be considered to produce a set of important effects that are native to reactive fluid mechanics. Most important results achieved by classical studies of this problem concerns the effect of geometry. For example, in the case $n=3$, it is possible to produce, for a unique set of parameters, infinitely many solutions, some of which are stable, and some that exhibit the phenomenon often called thermal runaway or, mathematically, finite time blow-up. These Gelfand type problems are attributed to many celebrated investigators: Barenblatt, Bratu, Emden, Fowler, Frank-Kamenetskii, Gelfand and Liouville [3]. There has been some notable recent interest in Gelfand type problems associated with thermal ignition theory. These problems are also associated with chemical reaction theory, radiative heat transfer, geometric and relativistic considerations in the Chandrasekhar model for an expanding universe and nanotechnology applications [2]. There are some good existence and uniqueness results as well as analytic solutions in special cases, see [1], [3], [4].

2.2 Alternate Formulations and an Example Problem

At present we are specifically examining the effect of coupling on chaos in the chemistry and fluid components. The Kuramoto-Sivashinsky equation is one important example of a different kind of model that applies for combustion among other physical problems. Sivashinsky developed the equation for modeling flame front instabilities and Kuramoto independently did so for the study of chemical turbulence. In sufficiently large domains, solutions have chaotic, or weakly turbulent, behavior [22]. Following [27], a classical 1D example is reproduced in Figure 3.

$$u_t = - \left(\frac{1}{2} u^2 \right)_x - u_{xx} - u_{xxxx}, \quad u(x, 0) = \cos \left(\frac{x}{16} \right) \left(1 + \sin \left(\frac{x}{16} \right) \right) \quad (16)$$

The 2D formulation of this problem in rectangular geometry:

$$u_t = \nu |\nabla u|^2 - \alpha u - \Delta u - \Delta^2 u \quad (17)$$

Or equivalently:

$$u_t = \nu (u_x^2 + 2u_x u_y + u_y^2) - \alpha u - u_{xx} - u_{yy} - u_{xxxx} - 2u_{xxyy} - u_{yyyy} \quad (18)$$

Our calculation is done using a straightforward implicit Crank-Nicolson scheme with central differences for all derivatives. A direct solve is performed at each time step, lagging the nonlinearity in uu_x resulting in

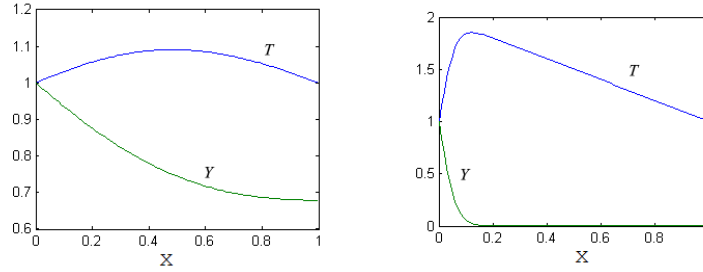


Figure 4: Reproduction of the example result presented in [8].

a penta-diagonal linear system. For historical references and the current state of the art on this problem, including simulations of chaotic solutions in 3D geometry, see [11].

2.3 Thermal Ignition and Chemical Coupling

If we assume a single chemical species, $Y(\vec{x}, t)$, freeze the mainflow such that $\vec{V}(\vec{x}, t) = 0$ and assume constant density, $\rho(\vec{x}, t) := \text{constant}$, then we have the nonlinear advection-reaction-diffusion model with one-step irreversible Arrhenius chemical kinetics :

$$\frac{\partial Y}{\partial t} = D\nabla^2 Y - \phi^2 Y e^{-\theta/T}, \quad \frac{\partial T}{\partial t} = \kappa \nabla^2 T + \beta \phi^2 Y e^{-\theta/T} \quad (19)$$

with constant parameters: $\kappa, D, \delta, A, \theta$. First we consider this problem in one spatial dimension following [8]. It is extended to an axisymmetric geometry and the periodic and aperiodic solutions are discovered. In this problem, the Lewis number (Le) is the non-dimensional ratio of mass to thermal diffusivity (k/D) and is known to significantly impact the numerical and physical results [24].

A direct comparison is made with [8], it is in excellent quantitative agreement with published results, showing (left) in the fast-reaction regime for $\theta = 10$ and (right) the slow-reaction regime for $\theta = 13.6$ in Figure 4. These are cases with steady state solutions that bound from above and below a reaction regime containing periodic and aperiodic solutions. In the 1D formulation $\nabla^2 := \partial^2/\partial x^2$ and the parameter regime of study is given by:

$$\beta = 4.287, \quad Le = 0.233, \quad \theta \in (12, 13), \quad \phi^2 = 70000 \quad (20)$$

subject to boundary conditions on the unit interval:

$$T(0) = 1, \quad T(1) = 1, \quad Y(0) = 1, \quad \frac{\partial Y(1)}{\partial x} = 0, \quad x = [0, 1] \quad (21)$$

Of particular importance, the bifurcation parameter, θ is the chemical activation energy. Note also that the maximum temperature in the field increases linearly with β . Examples are computed for $\theta = 12.61$ (left) and $\theta = 12.65$ (right) in Figure 5. Additionally a representative slice of the Y-T attractor space taken across the θ range is given in Figure 6. A unified picture of the Y-T attractor space which is a composite of representative θ locations produces the diagram in Figure 7. To extend the ignition problem, in the absence of fluid mechanics, to a 3D axisymmetric geometry we consider extensions of the same model given above to cylindrical coordinates:

$$\frac{\partial Y}{\partial t} = D \left(\frac{1}{r} \frac{\partial}{\partial r} \left(r \frac{\partial Y}{\partial r} \right) + \frac{\partial^2 Y}{\partial z^2} \right) - \phi^2 Y e^{-\theta/T}, \quad \frac{\partial T}{\partial t} = \kappa \left(\frac{1}{r} \frac{\partial}{\partial r} \left(r \frac{\partial T}{\partial r} \right) + \frac{\partial^2 T}{\partial z^2} \right) + \beta \phi^2 Y e^{-\theta/T} \quad (22)$$

For the boundary conditions, two representative models are considered, an insulated adiabatic wall model approximating submersion in a thermal bath, and a heated wall model approximating the spontaneous application of a heat source to one end of the experimental apparatus. The first model is a natural extension

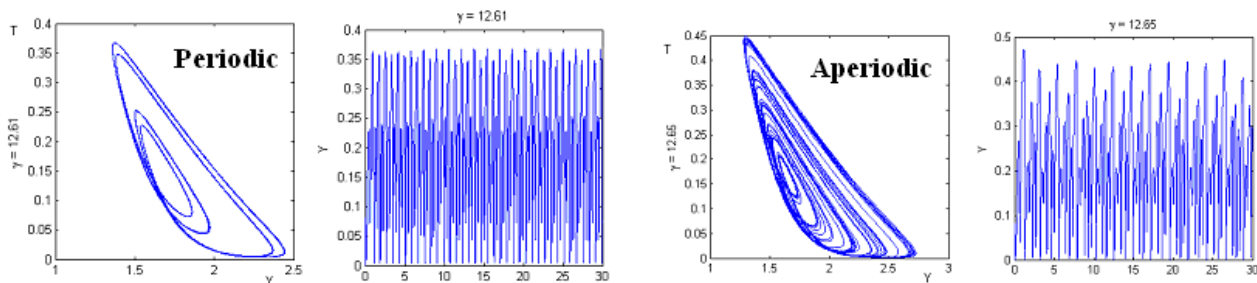


Figure 5: Premixed thermal ignition model periodic and aperiodic solutions.

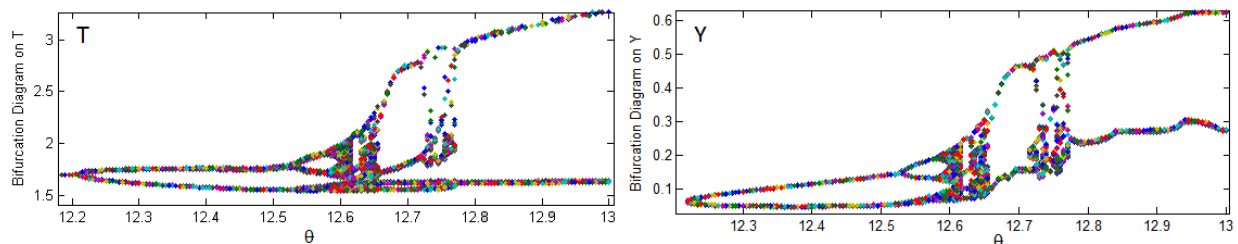


Figure 6: Bifurcation diagram of an attractor for a range of θ extracted from Eulerian point time series for heated wall (left) and thermal bath (right).

of the 1D model studied in [8], the second is chosen for similarity with [12], [18], [26]. In both cases we will use a line source of fuel along the axis of symmetry. The boundary conditions respectively are for $z \in [0, H/R]$, $r \in [0, 1]$ in the thermal bath model:

$$T(z = 0, r) = 1, T(z = H/R, r) = 1, T(z, r = 1) = 1, \frac{\partial T(z, r = 0)}{\partial r} = 0, \quad (23)$$

$$Y(z, r = 0) = 1, \frac{\partial Y(z = 0, r)}{\partial z} = 0, \frac{\partial Y(z, r = 1)}{\partial r} = 0, \frac{\partial Y(z = H/R, r)}{\partial r} = 0 \quad (24)$$

And, in the heated wall model:

$$T(z = 0, r) = 0, T(z = H/R, r) = 1, \frac{\partial T(z, r = 1)}{\partial r} = 0, \frac{\partial T(z, r = 0)}{\partial r} = 0, \quad (25)$$

$$Y(z, r = 0) = 1, \frac{\partial Y(z = 0, r)}{\partial z} = 0, \frac{\partial Y(z, r = 1)}{\partial r} = 0, \frac{\partial Y(z = H/R, r)}{\partial r} = 0 \quad (26)$$

Steady state examples of fast reaction profiles are computed for both the thermal bath case (left) and the heated wall case (right) in Figure 8.

3 Axisymmetric Swirling Incompressible Flow

Swirling the flow is a control technique whose main effects include considerably enhancing stability of most flames by creating toroidal recirculation zones facilitating mixing, decreasing combustion length through fluid entrainment, and even reducing maintenance costs on equipment [6]. A strongly swirling flow, sufficient to induce recirculation by vortex breakdown is needed to achieve these benefits. Vortex breakdown as a fluid mechanics problem has received extensive research attention [15]. Benchmarks for the steady cases and known chaotic dynamics in closely related problems will be studied for validation. The flow is axisymmetric which is a good assumption for many laminar flow cases [15]. There are three velocity components: radial (v_r), circumferential (w_θ), axial (u_z). First, assume ρ is time invariant and normalized to unity. Computing the standard coordinate transformation of the governing equations gives incompressible axisymmetric swirling

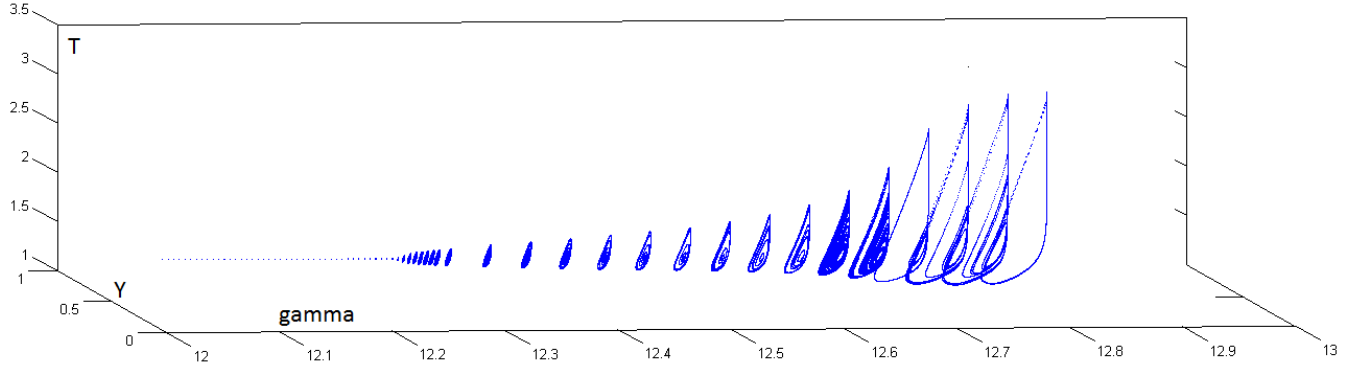


Figure 7: Period diagram extracted from the Y,T attractor space.

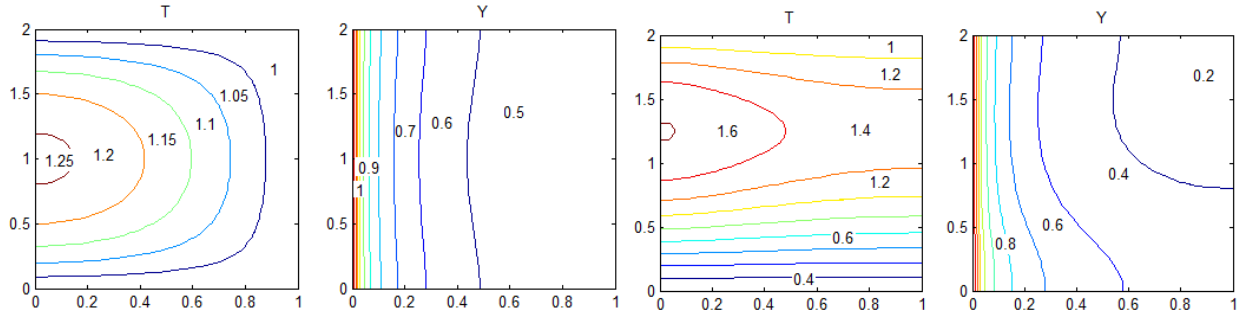


Figure 8: Thermal bath case (left) and the heated wall case (right) showing example steady state solutions for $H/R = 2$.

flow. Defined in non-conservative form in terms of stream function, vorticity and circulation as:

$$\begin{aligned}
 r \left(\frac{\psi_r}{r} \right)_r + (\psi)_{zz} &= -r\omega \\
 \omega_t + u\omega_r + w\omega_z - 2\frac{v v_z}{r} &= \frac{1}{Re} \left(\omega_{rr} + \frac{\omega_r}{r} + \omega_{zz} - \frac{\omega}{r^2} \right) \\
 v_t + uv_r + wv_z + \frac{uv}{r} &= \frac{1}{Re} \left(v_{rr} + \frac{v_r}{r} + v_{zz} - \frac{v}{r^2} \right)
 \end{aligned} \tag{27}$$

For the confined case we study a fixed cylinder with a rotating lid following the experimental apparatus of Escudier [9]. For the unconfined case, flow through a cylindrical domain is unconfined in the sense that there is a free stream boundary condition at $r = R$. The assumption of axisymmetry has been the subject of much debate. Some of the known issues outside the scope of this model include: asymmetric spiraling before vortex breakdown, asymmetric folding at downstream end of bubbles, and dye penetrating bubble interiors in experiments. Eulerian flow measures confirm that these inconsistencies have a small impact, except for studies involving Lagrangian particle dynamics, which should be modeled in 3D [28]. Following [21] the boundary conditions are:

$$\begin{aligned}
 \psi = v = \omega &= 0 \quad (r = 0, \quad 0 \leq z \leq H/R) \\
 \psi = v = 0, \quad \omega &= -\frac{1}{r} \frac{\partial^2 \psi}{\partial r^2} \quad (r = 1, \quad 0 \leq z \leq H/R) \\
 \psi = 0, v = r, \quad \omega &= -\frac{1}{r} \frac{\partial^2 \psi}{\partial z^2} \quad (z = 0, \quad 0 \leq r \leq 1) \\
 \psi = v = 0, \quad \omega &= -\frac{1}{r} \frac{\partial^2 \psi}{\partial z^2} \quad (z = H/R, \quad 0 \leq r \leq 1)
 \end{aligned} \tag{28}$$

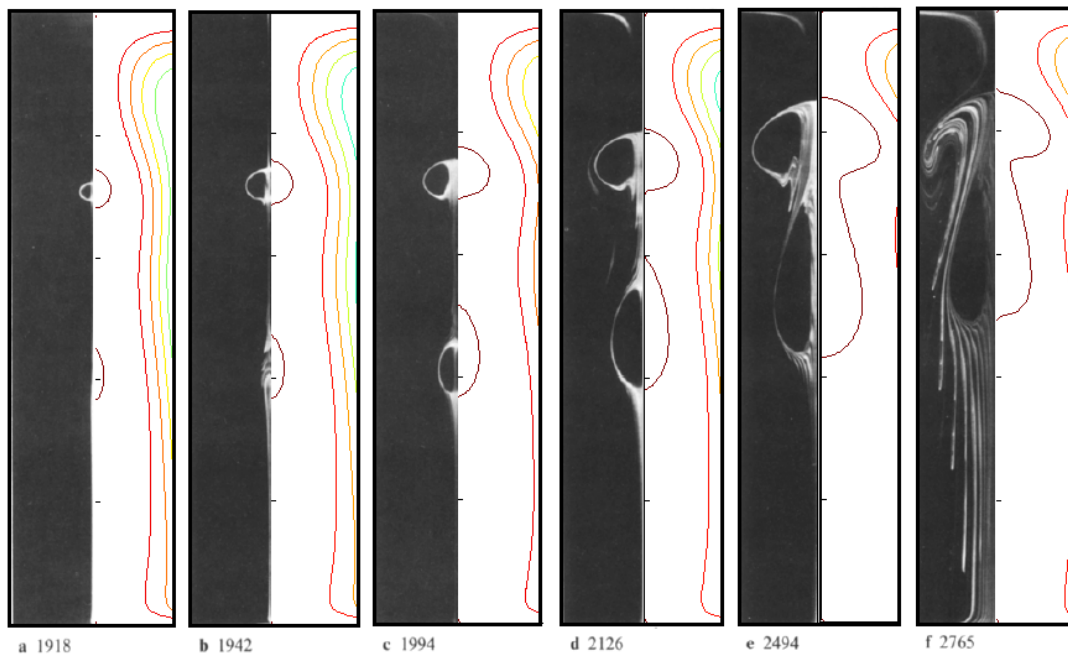


Figure 9: Direct comparison of numerical results with experiment data.

This problem has both periodic and aperiodic solutions depending, in particular, on the aspect ratio (Height/Radius) of the cylinder and the Reynolds number $\left(\frac{\Omega R^2}{\nu}\right)$ where Ω is the angular velocity, R is the radius and ν is the kinematic viscosity. In order to validate the code we make qualitative and quantitative comparisons following [9],[10]. For a qualitative comparison, in Figure 9, we compare with several experimental results for the set of Reynolds numbers of $\{1918, 1944, 1994, 2126, 2494, 2965\}$. Note that $Re = 2765$ is unsteady, and thus what is plotted is a time average of the stream function, in this case from time 750 to 1000. Qualitatively the agreement seems quite reasonable with particular emphasis placed on the location of vortex breakdown. We also make a comparison with [10] in Figure 10. One feature not shown at this level of resolution are the corner Moffatt eddies. This phenomena is well known for confined flows of this type [19]. To make the comparison more rigorous, following the example set forth in [10], we make the following quantitative analysis detailing the nondimensional location of the stagnation points along the z -axis for $r = 0$ in Figure 11. Here the coarsest mesh is 21×41 and the finest mesh is 151×301 . In all cases $\Delta x = \Delta r$, although this is not necessary. One observes that the qualitative behavior of the solutions does not appear particularly sensitive to the grid, although the precise location of the breakdown, at least in this is example, can vary by 15% or more from a reasonably coarse mesh to a finer one. Measuring the photographs from [9] which gave this result for only the uppermost stagnation point, as well as using the graphs in [10], it is estimated the steady-state location of the vortex breakdown in the case $Re = 1854$, $H/R = 2$, should be $x_{s_1} \approx 0.21124$. Fitting a fourth degree polynomial to the last four points in our data set our estimate would be $x_{s_1} \approx 0.2109$ for an error of 0.16%. Another quantitative comparison is available from [21] which reports maximum and minimum values for the stream function, circulation and vorticity fields. This is reported here:

Re	Present				Lopez (1990)			
	min(ψ)	max(ψ)	min(ω)	max(ω)	min(ψ)	max(ψ)	min(ω)	max(ω)
1918	-8.00E-03	4.54E-06	-3.76	15.9	-7.90E-03	1.00E-06	-3.80	15.6
1942	-7.98E-03	7.85E-06	-3.77	16.0	-7.90E-03	2.80E-06	-3.80	15.7
1994	-7.92E-03	1.58E-05	-3.81	16.2	-7.80E-03	8.80E-06	-3.80	15.8
2126	-7.78E-03	3.80E-05	-3.90	16.6	-7.60E-03	3.00E-05	-3.90	18.2
2494	-7.42E-03	2.63E-05	-4.11	17.7	-7.30E-03	7.40E-05	-4.40	17.2
2765	-7.68E-03	2.61E-04	-4.36	18.5	-7.00E-03	8.60E-05	-4.70	17.8

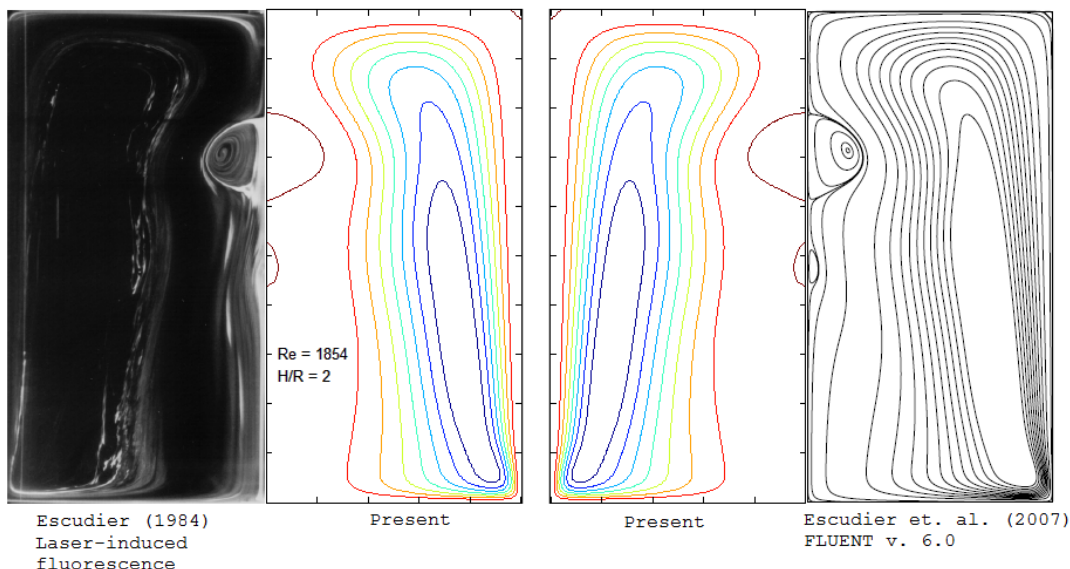


Figure 10: Steady state, $Re = 1854$, $H/R = 2$.

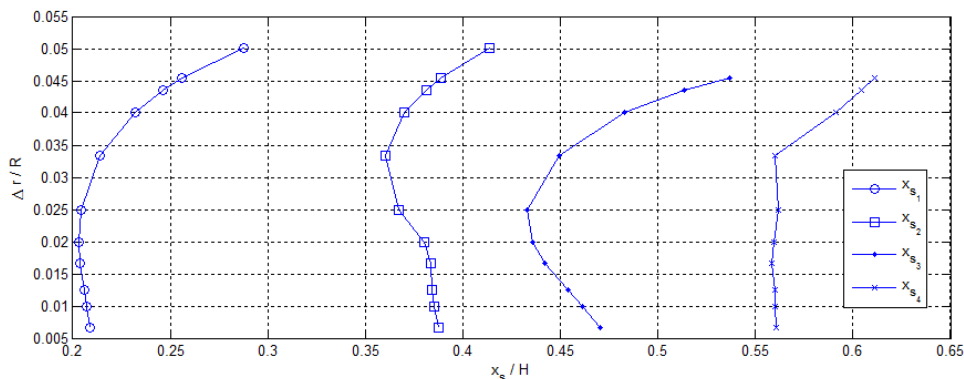


Figure 11: Location of onset points where z -axial velocity changes sign. In this case there are 4 with s_1 closest to the lid in order to s_4 which is farthest.

The agreement is not perfect, but they are quantitatively similar. Our table is generated using a grid resolution of 61×151 , where $H/R = 2.5$. The unsteady case of $Re = 2765$ is generated using a time average this time from 1000 to 1500.

It is found by numerical experiment that the flow solutions are numerically stable up to Reynolds numbers as high as 14,750 (in the case of $H/R = 2$) for several thousand time steps. A more detailed analysis has been conducted for Reynolds numbers in the range of 2000 to 6000 in increments of 100 using a grid with $\Delta x \approx \Delta r \approx 0.02$. The largest Lyapunov exponent (LLE) is computed from the $\|\psi\|_2$ time series by a modified method similar to that given in [29]. The main differences being that at each iteration a new fiducial point is selected at random from the attractor, and instead of choosing a single point near this base point, then a cloud of nearby points is selected and evolved in time to better estimate the local attractor expansion. The results are summarized in Figure 12 showing plots of the LLE's generated from the time history of $\|\psi\|_2$ for time from 1000 to 2000, allowing 1000 time units for transients to decay between samples. Rather than starting each new Reynolds number case from the quiescent initial conditions, the input for the next Reynolds number is taken as the solution at time $t = 2000$ from the previous Reynolds number case. It is remarked that this method of generating the time series might affect the results if insufficient

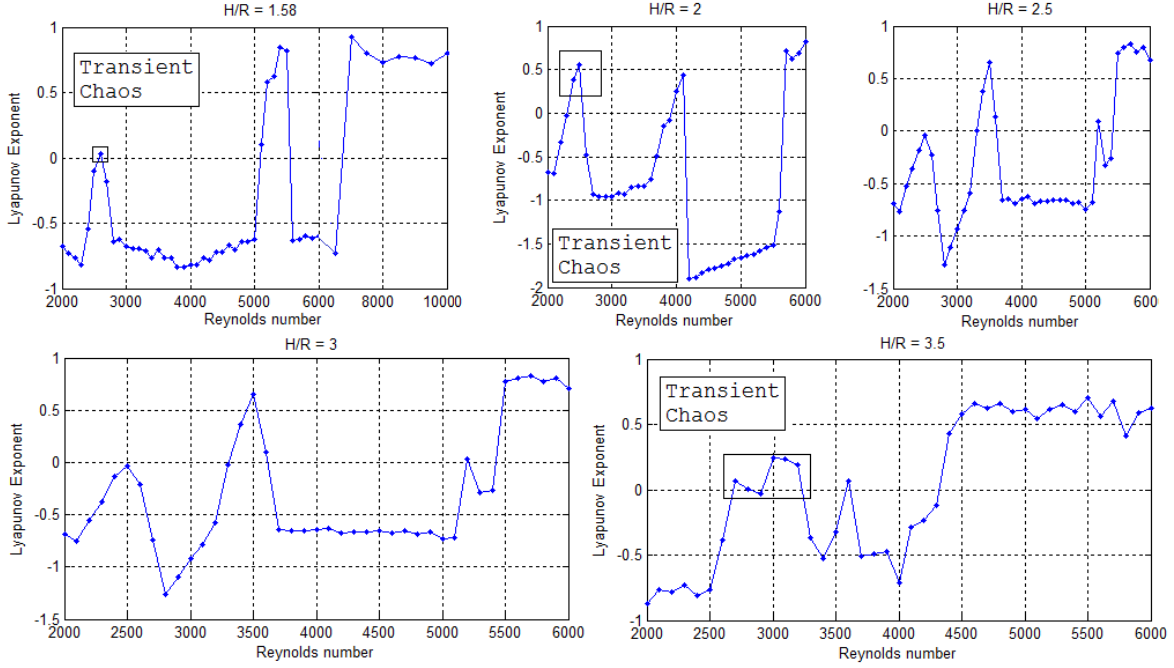


Figure 12: Largest Lyapunov Exponent for $H/R = 1.58, 2, 2.5, 3, 3.5$ from left to right, top to bottom. Transient chaos is labeled.

time was given to let transient solutions decay, or multiple solutions exist. Also, in cases where the $\|\psi(t)\|_2$ by $\|\psi(t + \Delta t)\|_2$ attractor has a high number of folds calculation of the Lyapunov exponent is questionable. In this case, comparison with a Poincare section as well as the power spectral analysis are used to overrule this prediction. A vortex pinch-off as well as some irregular breakdown structures have been observed, these are reported in Figure 13. In addition to this, several vortex shapes were observed beyond the classical experimentally produced configurations. These are shown in Figure 14.

Numerical methods and Initial conditions For the case without temperature and chemical effects impulsive start is used for most simulations. The exception is that the high Reynolds number simulations ran one case into the next without resetting the initial condition. The main aspects of the numerical procedure for a problem of this type are the time stepping scheme, treatment of the nonlinear terms and the discretization of the advection terms. A long time, high resolution, integration is desirable. For this task an explicit Arakawa method is used. To study unsteady behavior, the output is desired at many intermediate time values, hence the benefit of a large time step from an implicit method is lost. In addition, the conservation properties of the Arakawa method are important. Recall, as proved in [20], the Arakawa method is equivalent to a finite element method and preserves conservation laws for mean vorticity, mean square vorticity and kinetic energy.

Arakawa's scheme for the advection terms is given by:

$$\begin{aligned}
 J(\zeta) = & \frac{-1}{12\Delta x\Delta r} [(\psi_{i,j-1} + \psi_{i+1,j-1} - \psi_{i,j+1} - \psi_{i+1,j+1})(\zeta_{i+1,j} - \zeta_{i,j})\dots \\
 & + (\psi_{i-1,j-1} + \psi_{i,j-1} - \psi_{i-1,j+1} - \psi_{i,j+1})(\zeta_{i,j} - \zeta_{i-1,j})\dots \\
 & + (\psi_{i+1,j} + \psi_{i+1,j+1} - \psi_{i-1,j} - \psi_{i-1,j+1})(\zeta_{i,j+1} - \zeta_{i,j})\dots \\
 & + (\psi_{i+1,j-1} + \psi_{i+1,j} - \psi_{i-1,j-1} - \psi_{i-1,j})(\zeta_{i,j} - \zeta_{i,j-1})\dots \\
 & + (\psi_{i+1,j} - \psi_{i,j+1})(\zeta_{i+1,j+1} - \zeta_{i,j}) + (\psi_{i,j-1} - \psi_{i-1,j})(\zeta_{i,j} - \zeta_{i-1,j-1})\dots \\
 & + (\psi_{i,j+1} - \psi_{i-1,j})(\zeta_{i-1,j+1} - \zeta_{i,j}) + (\psi_{i+1,j} - \psi_{i,j-1})(\zeta_{i,j} - \zeta_{i+1,j-1})]
 \end{aligned} \tag{29}$$

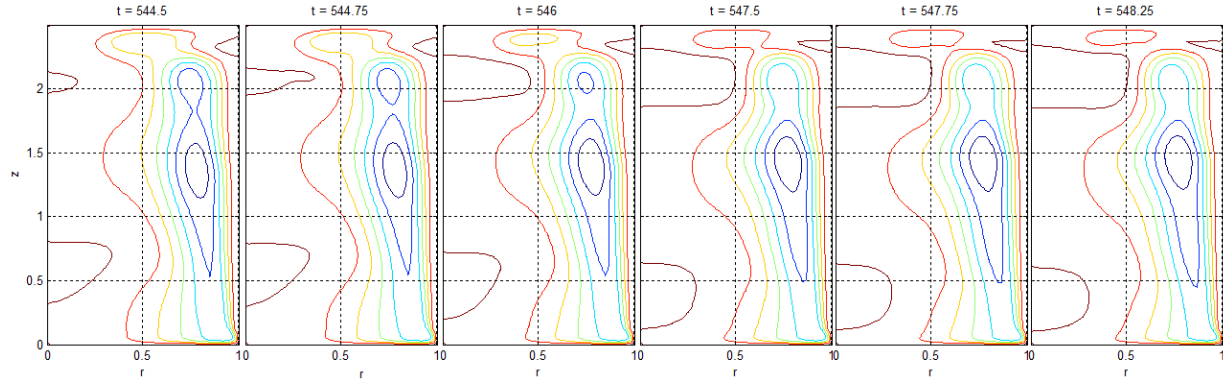


Figure 13: Pinch-off phenomena observed in unsteady simulation at $H/R = 2.5$, $Re = 6000$.

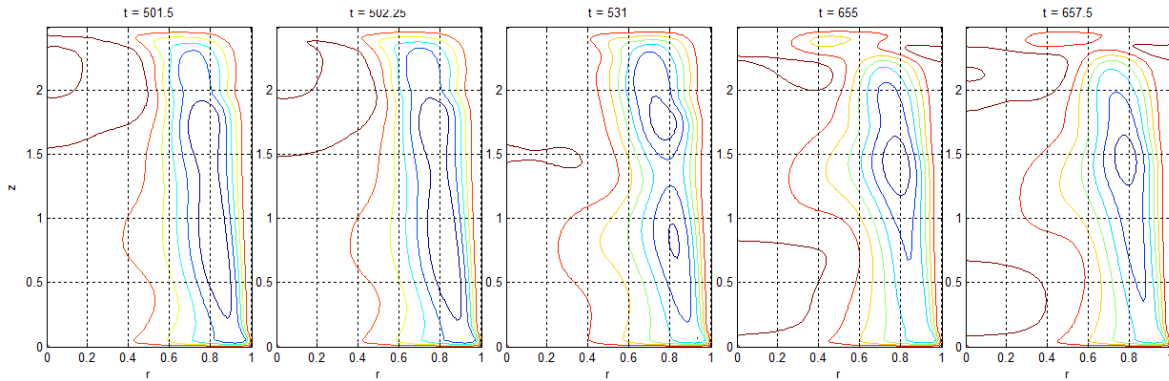


Figure 14: Examples of other observed phenomena at $H/R = 2.5$, $Re = 6000$.

Here, the operator J is defined as:

$$J = \frac{\partial \psi}{\partial z} \frac{\partial}{\partial r} - \frac{\partial \psi}{\partial r} \frac{\partial}{\partial z} \quad (30)$$

The advection terms in the ω, v equations are discretized according to:

$$\begin{aligned} \omega_t - J\left(\frac{\omega}{r}\right) - 2\frac{v\omega_z}{r} &= \frac{1}{Re} \left(\omega_{rr} + \frac{\omega_r}{r} + \omega_{zz} - \frac{\omega}{r^2} \right) \\ v_t - \frac{1}{r}J(v) + \frac{uv}{r} &= \frac{1}{Re} \left(v_{rr} + \frac{v_r}{r} + v_{zz} - \frac{v}{r^2} \right) \end{aligned} \quad (31)$$

With temperature effects and chemical species, the advection transport terms in the T, Y equations respectively will be in the same form as the equation for v above. The explicit predictor-corrector algorithm is:

$$\frac{\bar{u} - u^n}{\Delta t} = f(u^n), \quad \frac{u^{n+1} - u^n}{\Delta t} = \frac{1}{2}f(u^n) + \frac{1}{2}f(\bar{u}) \quad (32)$$

This method is similar to that used by Lopez in [21].

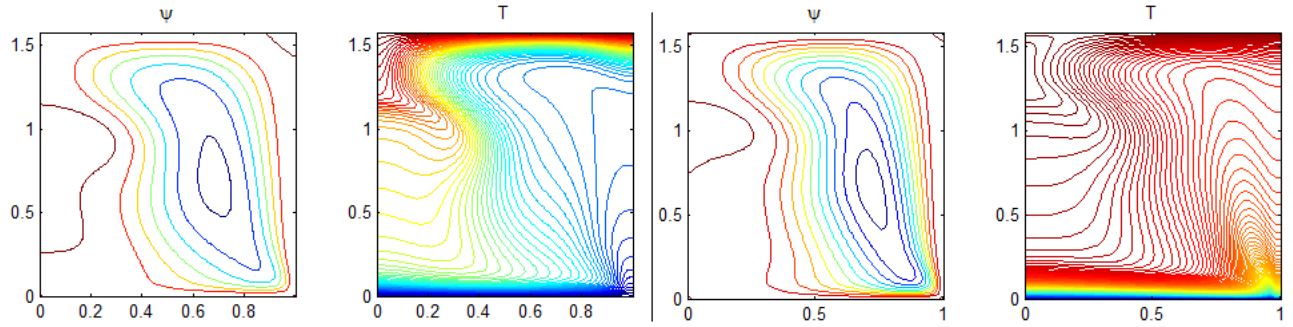


Figure 15: Steady state, $Re = 1350$, $H/R = 1.58$, $Ec = 0.1$ (left), $Ec = 4.0$ (right), and for both $Pr = 0.7$, $Ra = -0.05$.

3.1 Incompressible flow with and without chemical coupling using Boussinesq approximation

The dimensionless initial boundary value problem is given in terms of the Prandtl Number (Pr), Rayleigh number (Ra), Eckert number (Ec) and Reynolds number (Re), see [18], [26]:

$$\begin{aligned}
 r \left(\frac{\psi_r}{r} \right)_r + \psi_{xx} &= r\omega \\
 \omega_t + u\omega_r + w\omega_z - 2\frac{v\omega_z}{r} &= -Ra T_r + \frac{1}{Re} \left(\omega_{rr} + \frac{\omega_r}{r} + \omega_{zz} - \frac{\omega}{r^2} \right) \\
 v_t + uv_r + wv_z + \frac{uv}{r} &= \frac{1}{Re} \left(v_{rr} + \frac{v_r}{r} + v_{zz} - \frac{v}{r^2} \right) \\
 T_t + uT_r + wT_z &= \frac{1}{Pr \cdot Re} \left(T_{rr} + \frac{T_r}{r} + T_{zz} \right) \dots \\
 &\dots + \frac{Ec}{Re} \left(2 \left(u_r^2 + \frac{u^2}{r^2} + w_z^2 \right) + \left(v_r - \frac{v}{r} \right)^2 + (u_z + w_r)^2 \right)
 \end{aligned} \tag{33}$$

A heated wall model boundary condition on temperature is first used to compare with published results:

$$T(z = 0, r) = 1, T(z = H/R, r) = 0, \frac{\partial T(z, r = 1)}{\partial r} = 0, \frac{\partial T(z, r = 0)}{\partial r} = 0 \tag{34}$$

Note that this model forces a thermal gradient. In contrast to this, in the thermal bath model, where quiescent uniformly $T(x, r) = 1$ initial condition is used, the case where $Da = 0$ produces flow solutions equivalent to $Ra = 0$. For the heated wall model, our results are in qualitative agreement with [18] and [26] as shown in Figure 15. It is found the Eckert number, governing the viscous dissipation, diminishes vortex breakdown effects as shown in Figure 16. Note also in 16 the corner Moffatt eddies are large and their size is shown to depend on the Eckert number. When studying chaotic solutions, and in light of using a Boussinesq approximation, including $Ec > 0$ is found to provide a stabilizing effect that has a tendency to reduce the sensitivity of the mainflow to T_r . In this model several effects are observable. It is observed that decreasing the Rayleigh number enhances the vortex breakdown effect as shown in Figure 17. Note the direction of the temperature gradient is from bottom, at $z = 0$, to top, at $z = H/R$, in the heated wall model. If the direction is reversed, then increasing the Rayleigh number will have a similar effect. Through varying only the Prandtl number for example to 7.1, with $Ra = -0.05$, $Ec = 0$, $H/R = 2$, $Re = 1854$, $Da = 0$, this model can produce persistent chaotic oscillations. An example showing $\|\psi\|_2$ time series is shown up to $t = 5000$ in Figure 18. Here the largest Lyapunov exponent is approximately 0.657. In this case when $Ra = -0.01$ a steady state solution is reached with a chaotic transient largely decayed by $t \approx 500$. When $Pr = 0.7$ and $Ra = -0.05$ a steady state solution exists, but it takes until $t \approx 2000$ for the regular periodic oscillations to largely decay. These results are shown in Figure 19.

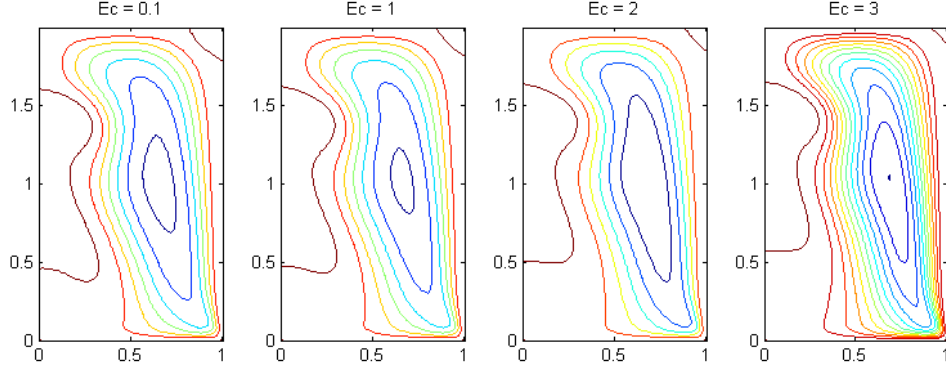


Figure 16: $\|\psi\|_2$ steady state for $Ra = -0.05$, $Pr = 7.1$, dependence on $Ec = 0.1, 1, 2, 3$, $H/R = 2$, $Re = 1854$.

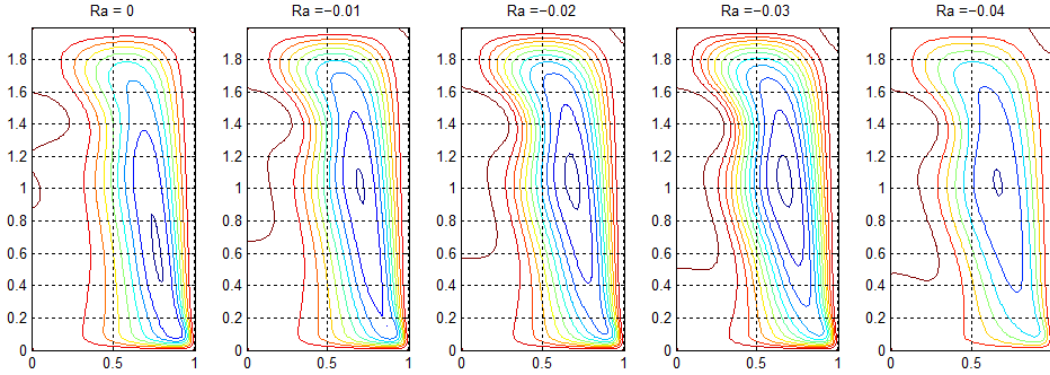


Figure 17: Swirling flow with temperature effect coupled through Ra for $H/R = 2$, $Re = 1854$, $Pr = 0.7$, $Ec = 0$, and heated wall boundary conditions for T .

We extend this model to include a chemical reaction. The Boussinesq approximation is used coupling the fluid mechanics and chemistry proportional to a gradient of temperature in the radial direction. According to the Boussinesq approximation, the density is not constant, but the underlying cause is temperature, not pressure. In this case there is weak coupling between the fluid dynamics and chemistry, but the temperature effect is decoupled from the pressure effect. The non-dimensional governing equations are:

$$\begin{aligned}
 r \left(\frac{\psi_r}{r} \right)_r + (\psi)_{zz} &= -r\omega \\
 \omega_t + u\omega_r + w\omega_z - 2\frac{v v_z}{r} &= \frac{1}{Re} \left(\omega_{rr} + \frac{\omega_r}{r} + \omega_{zz} - \frac{\omega}{r^2} \right) \\
 v_t + uv_r + wv_z + \frac{uv}{r} &= -RaT_r + \frac{1}{Re} \left(v_{rr} + \frac{v_r}{r} + v_{zz} - \frac{v}{r^2} \right) \\
 Y_t + uY_r + wY_z &= \frac{1}{Sc \cdot Re} \left(Y_{rr} + \frac{Y_r}{r} + Y_{zz} \right) - D_a Y e^{-\theta/T} \\
 T_t + uT_r + wT_z &= \frac{1}{Pr \cdot Re} \left(T_{rr} + \frac{T_r}{r} + T_{zz} \right) + \beta D_a Y e^{-\theta/T}
 \end{aligned} \tag{35}$$

where:

$$u = \frac{\psi_r}{r}, \quad v = -\frac{\psi_x}{r} \tag{36}$$

In the limit where $Ra = 0$, the fluid mechanics and the chemical thermodynamics are completely decoupled. Note that in all cases we will take $Sc = 1$. In addition, we will now introduce species and thermal bath

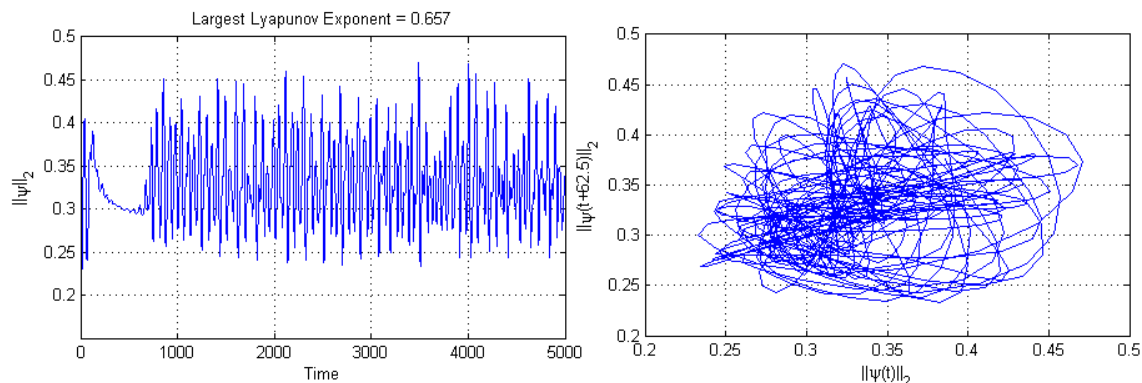


Figure 18: Sustained chaotic $\|\psi\|_2$ oscillations for $Ra = -0.05$, $Pr = 7.1$, $Ec = 0$, $H/R = 2$, $Re = 1854$, $Da = 0$. The Poincaré section on the right is produced using $t \in [2500, 5000]$.

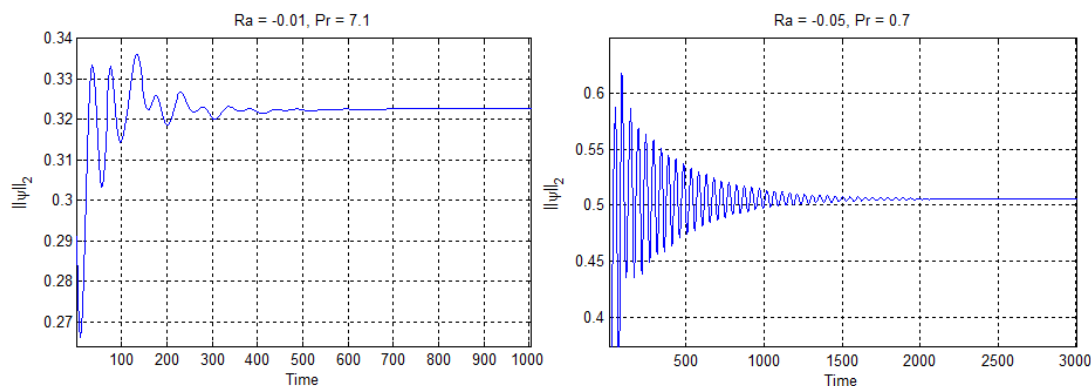


Figure 19: Steady state $\|\psi\|_2$ achieved with $H/R = 2$, $Re = 1854$, $Ec = 0$, $Da = 0$ for $Ra = -0.01$, $Pr = 7.1$ (left) and $Ra = -0.05$, $Pr = 0.7$ (right).

boundary conditions:

$$T(z = 0, r) = 1, T(z = H/R, r) = 1, T(z, r = 1) = 1, \frac{\partial T(z, r = 0)}{\partial r} = 0, \quad (37)$$

$$Y(z, r = 0) = 1, \frac{\partial Y(z = 0, r)}{\partial z} = 0, \frac{\partial Y(z, r = 1)}{\partial r} = 0, \frac{\partial Y(z = H/R, r)}{\partial r} = 0 \quad (38)$$

Note that $Da = 0$ is equivalent to $Ra = 0$ in this case. The combustion can have a variety of effects, both stabilizing and destabilizing. For example, a strong reaction process can cause the solution to quickly approach a steady state as shown in Figure 20. In this figure, the rightmost plots are of the case where $Ra = 0$ and are a time average of the periodic solution from $t = 1000$ to 1500 . In this case, with fixed $H/R = 2.5$, $Re = 2765$, and thermal bath B.C. for T with $Ra = 0.05$, it is seen that varying the Prandtl number and the combustion variables, Da , θ , and β , the non-reactive flow transitions from unsteady to steady. The steady state is also shown to depend on the Prandtl number and reaction strength. The Rayleigh number, Ra , plays an important role in the Boussinesq approximation. In Figures 21 and 22, which are different plots of the same flow simulation, the Rayleigh number effect is specifically investigated for reactive flow with thermal bath boundary conditions. In all these cases: $H/R = 2$, $Re = 1854$, $Pr = 0.01$, $Ec = 0$, $Sc = 1$, $Da = 1$, $\beta = 4$, $\theta = 3$ and $Ra = [-0.1, -0.05, 0, 0.05, 0.1]$. It is observed that vortex breakdown structure and temperature and species concentration maxima are sensitive to varying Ra .

Another important effect is that combustion alone is enough to induce strong periodic and aperiodic behavior from an otherwise steady state solution as shown in Figure 23. This figure also shows how Da can affect

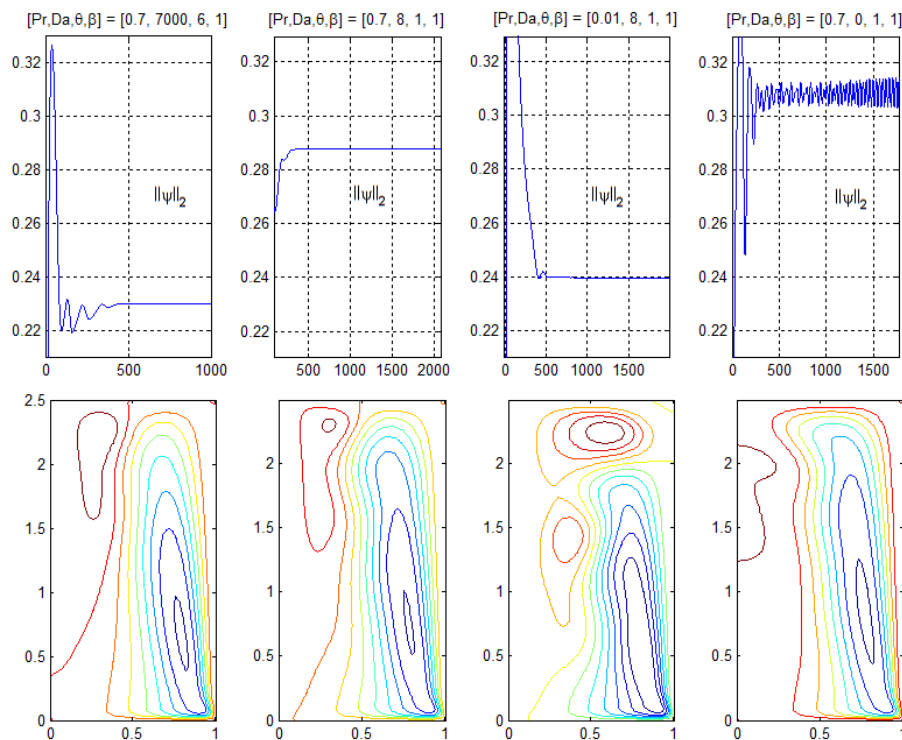


Figure 20: $H/R = 2.5$, $Re = 2765$, showing stabilizing effect on mainflow for several combustion processes.

the oscillatory behavior. Here, at a relatively low Reynolds number, $Re = 1854$, there is a steady solution for $Da = 0$, $Ra = -0.05$ and it is very similar to that shown in Figure 17 for $Ra = -0.04$. Note $\|\psi\|_2 \approx 0.5$ at steady state. In this case, the base is $H/R = 2$, $Re = 1854$, $Ec = 0$, $Ra = -0.05$, using the heated wall boundary conditions for temperature produces a periodic oscillatory solution. Further increase of Da results in a chaotic solution. $Ec > 0$ damps the aperiodicity out of the solutions, however, further increasing Da can bring about aperiodic solutions even with the viscous dissipation effect.

Combustion can also dramatically change the startup transient behavior as shown in Figure 24. The long time periodic behavior of the two solutions are also shown side-by-side for comparison in segments of $t \in \{[0, 1000], [1000, 2500], [2500, 4000]\}$ in Figure 24. In these plots $H/R = 2$, $Re = 4500$, $Ec = 0$, $Pr = 0.7$, $Ra = 0.1$, with thermal bath B.C. for T , showing $\|\psi\|_2$ for $Da = 8$, $\beta = 1$, $\theta = 1$. In one case the solution very quickly approaches a periodic solution, while in the other transient chaos persists for many time steps.

In fully chaotic cases, where aperiodicity is not destroyed by the chemical coupling, combustion can cause a finer time scale to present. This phenomena is shown in Figure 25 for a case with heated wall boundary conditions. In one case $Da = 0$, in the other $Da = 1$ while all other parameters are given by: $H/R = 2$, $Re = 4500$, $Pr = 0.7$, $Ra = -0.05$, $Da = 1$, $\Theta = 1$, $\beta = 1$, $Ec = 0.1$. The case with combustion, the Lyapunov exponent for the $\|\psi\|_2$ time series is $LLE \approx 0.596$, and without where $Da = 0$, $LLE \approx 0.480$. In addition, the power spectra for $\|\psi\|_2$ is shown in Figure 25 with $Da = 0$ on the left and $Da = 1$ on the right. As expected, the presence of a second finer time scale shows a denser high frequency response. Extending what was shown above, it is also observed that the Raleigh number effect can change the amplitude of oscillations in a chaotic time series as well as the long term mean values. These phenomena are shown in Figure 26 for $\|\psi\|_2$ and $\|T\|_2$ time series. All cases are proven chaotic by calculation of the largest Lyapunov exponent (LLE). $Ra = 0$ and $Ra = 0.1$ have similar $LLE \approx 0.64, 0.63$ respectively, while the case of $Ra = -0.1$ has slightly high $LLE \approx 0.802$.

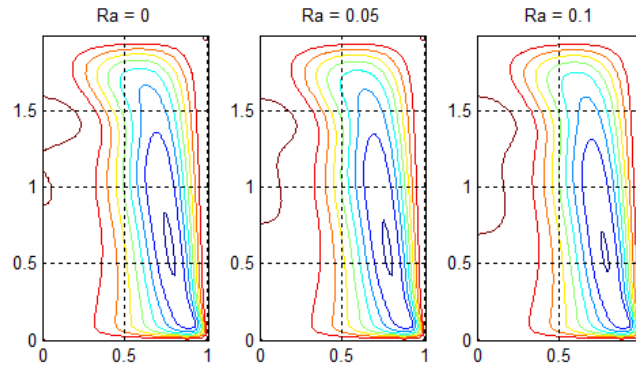


Figure 21: Streamlines showing location of vortex breakdown for variable $Ra = [-0.1, -0.05, 0, 0.05, 0.1]$ for $H/R = 2$, $Re = 1854$, $Pr = 0.01$, $Ec = 0$, $Sc = 1$, $Da = 1$, $\beta = 4$, $\theta = 3$ with thermal bath boundary conditions.

Most importantly perhaps, the presence of combustion, even weak combustion, can change the periodicity of the solution. For example, as shown in Figure 27 a periodic solution without combustion becomes aperiodic with combustion. In this figure, $H/R = 2$, $Re = 5500$, $Ec = 0$, $Pr = 0.7$, $Da = 1$, $\theta = 3$, $\beta = 4$ along with thermal bath boundary conditions for temperature. In one case $Ra = 0$ and, in the other, $Ra = -0.05$.

Numerical methods and Initial conditions This problem can be stiff for certain parameter range. Rather than using one fine time scale, a two-timing procedure is used. The time scale of the temperature and species equation, Δt_{chem} , is determined by trial and error necessarily finer than the fluid dynamics problem alone. The numerical procedure is to advance the stream function, velocity fields, swirl and vorticity Δt . Note that a direct solver is used to advance the stream function. Hereafter the temperature and species equations are advanced Δt on a finer time scale $\Delta t_{chem} = \frac{\Delta t}{k}$, $k \in \mathbb{Z}$. Then the process is repeated. In our simulations these values ranged from $k = 1$ to $k = 1000$. The numerical stability constraint on Δt_{chem} was determined by trial and error.

3.2 Compressible flow with chemical coupling

At present we consider only steady state cases of the compressible reactive flow. In this case, transient solutions achieved during numerical convergence are nonphysical, however, the steady state results should be valid. Note that the stream function-vorticity-circulation model, as written, could not be adapted without

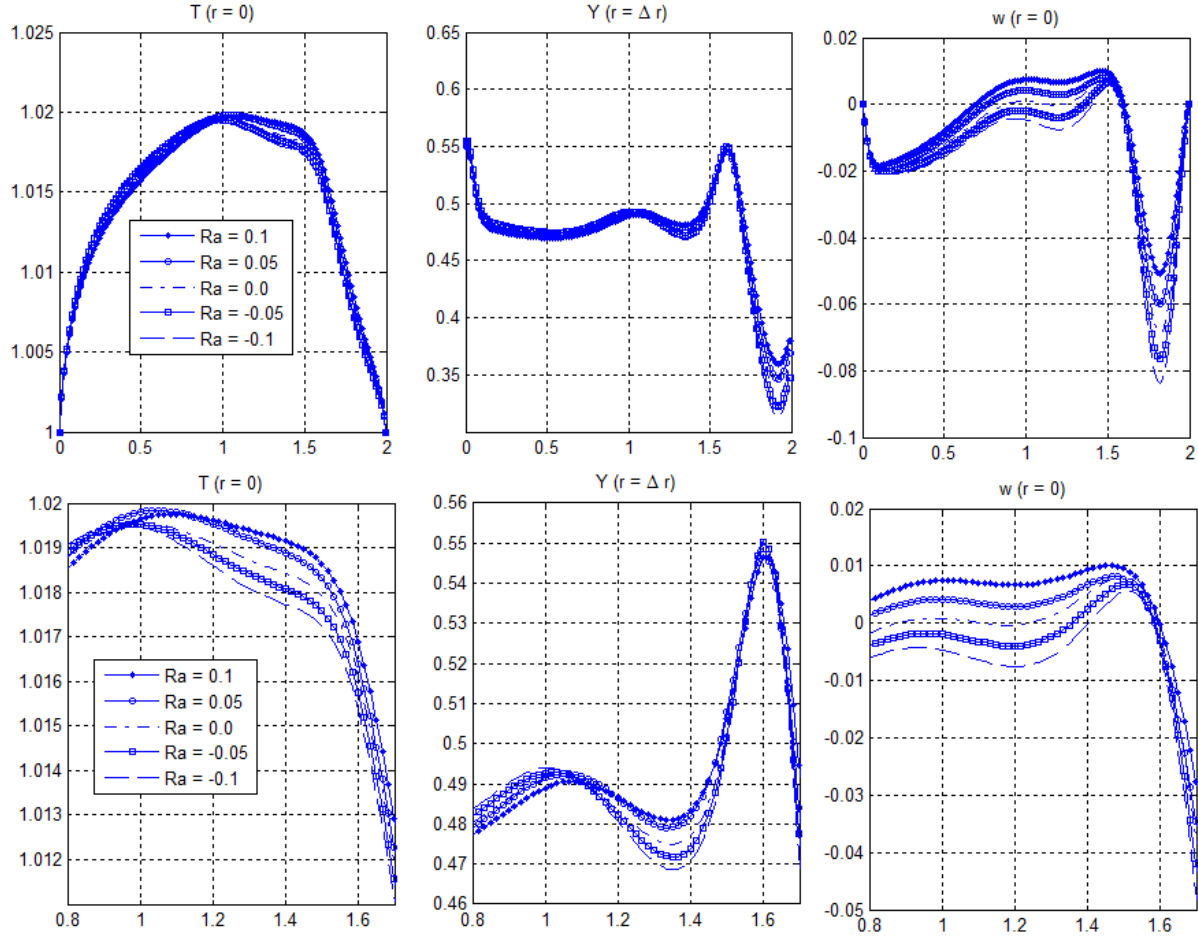


Figure 22: T at $r = 0$ (left), Y at $r = \Delta t$ (center) and w at $r = 0$ (right) in the region of vortex breakdown for $Ra = [-0.1, -0.05, 0, 0.05, 0.1]$ for $H/R = 2$, $Re = 1854$, $Pr = 0.01$, $Ec = 0$, $Sc = 1$, $Da = 1$, $\beta = 4$, $\theta = 3$ with thermal bath boundary conditions.

modifications to the unsteady case. The unsteady non-dimensional model is:

$$\begin{aligned}
 \frac{1}{r} (r\rho\phi_r)_r + (\rho\phi_z)_z &= -\rho_t, & r \left(\frac{1}{\rho} \frac{\psi_r}{r} \right)_r + \left(\frac{\psi}{\rho} \right)_{zz} &= -r\omega \\
 \rho\omega_t + \rho u\omega_r + \rho w\omega_z - 2\frac{v v_z}{r} &= \frac{1}{Re} \left(\omega_{rr} + \frac{\omega_r}{r} + \omega_{zz} - \frac{\omega}{r^2} \right) \\
 \rho v_t + \rho u v_r + \rho w v_z + \frac{u v}{r} &= -Ra T_r + \frac{1}{Re} \left(v_{rr} + \frac{v_r}{r} + v_{zz} - \frac{v}{r^2} \right) \\
 \rho Y_t + \rho u Y_r + \rho w Y_z &= \frac{1}{Sc \cdot Re} \left(Y_{rr} + \frac{Y_r}{r} + Y_{zz} \right) - Da \rho Y e^{-\theta/T} \\
 \rho T_t + \rho u T_r + \rho w T_z &= \frac{1}{Pr \cdot Re} \left(T_{rr} + \frac{T_r}{r} + T_{zz} \right) + \beta Da \rho Y e^{-\theta/T} \\
 \rho &= \frac{p}{T} \frac{\gamma}{\gamma - 1}, & \Delta p &= \nabla \left(\rho V_t + \rho V \cdot \nabla V - \frac{1}{Re} \left[\nabla^2 V + \frac{1}{3} \nabla(\nabla \cdot V) \right] \right)
 \end{aligned} \tag{39}$$

where by a Helmholtz type decomposition:

$$w = \phi_z + \frac{\psi_r}{r\rho}, \quad u = \phi_r - \frac{\psi_x}{r\rho} \tag{40}$$

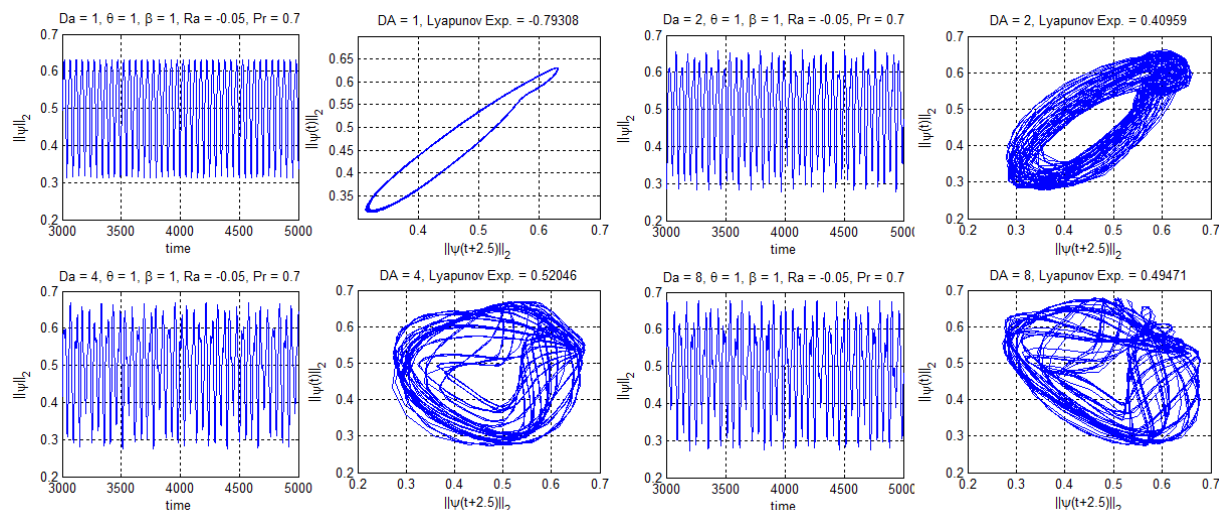


Figure 23: $H/R = 2$, $Re = 1854$, $Ec = 0$, $Ra = -0.05$, $\Theta = 1$, $\beta = 1$, heated wall B.C. for T , we see $\|\psi\|_2$ time series (Left) $Da = 1.0$, $LLE \approx -0.79$, (Left middle) $Da = 2$, $LLE \approx 0.41$, (Right middle) $Da = 4$, $LLE \approx 0.52$, (Right) $Da = 8$, $LLE \approx 0.49$.

For modeling purposes it might be useful to make a constant pressure assumption. In general a Poisson equation for the pressure will need to be solved. For the steady flow results we take $\phi = 0$. A code has been developed and validated for the non-reactive case following [13]. The problem considered is axisymmetric flow in a cylindrical geometry with a steady, continuous, vortex generated at the inlet. Comprehensive results, in the absence of combustion, have been reproduced quantitatively matching those reported in [13]. The model has been extended to include combustion in the compressible reactive case. A preliminary test case for small heat release with constant pressure has been calculated and is shown in Figure 28. In addition to producing a larger bubble, vortex breakdown develops sooner with the presence of this weak combustion process, which matches the conclusions presented in [7], as shown in Figure 29. Additionally, it is observed that the mixing due to vortex breakdown greatly affects the temperature such that a local temperature maximum is coincident with a vortex bubble center. Extension to unsteady flow with chaotic dynamics will be the subject of future research. Some recent work in this area has been undertaken in [14].

4 Conclusions

Present chaotic behavior of the solution of the thermal ignition problem is in agreement with published results [8]. Present incompressible fluid mechanics results for the case of confined flow and compressible results for unconfined flow are in agreement with published results [18],[13],[26]. In this study chaotic dynamics in reactive swirling has been investigated. It has been found that combustion can be a stabilizing and destabilizing force. Reactions can introduce fine time scales that can change the solution dramatically. Coupling through the Ra and combustion parameters are very influential. Reactive processes can greatly affect the startup conditions as well as persistent behavior of the system. It is also found that the flow solution is very sensitive to changes in temperature as demonstrated by the very strong influence of the Rayleigh number through the Boussinesq approximation. Chemical reaction affects the results qualitatively and quantitatively. The axisymmetric model used in the present calculations is sufficient for many applications however, one criticism of the current approach is that symmetry might be broken by the microscale introduced in the chemical reaction, hence a 3D approach would be necessary [28]. Advanced computational resources are also required for the turbulent flow calculations.

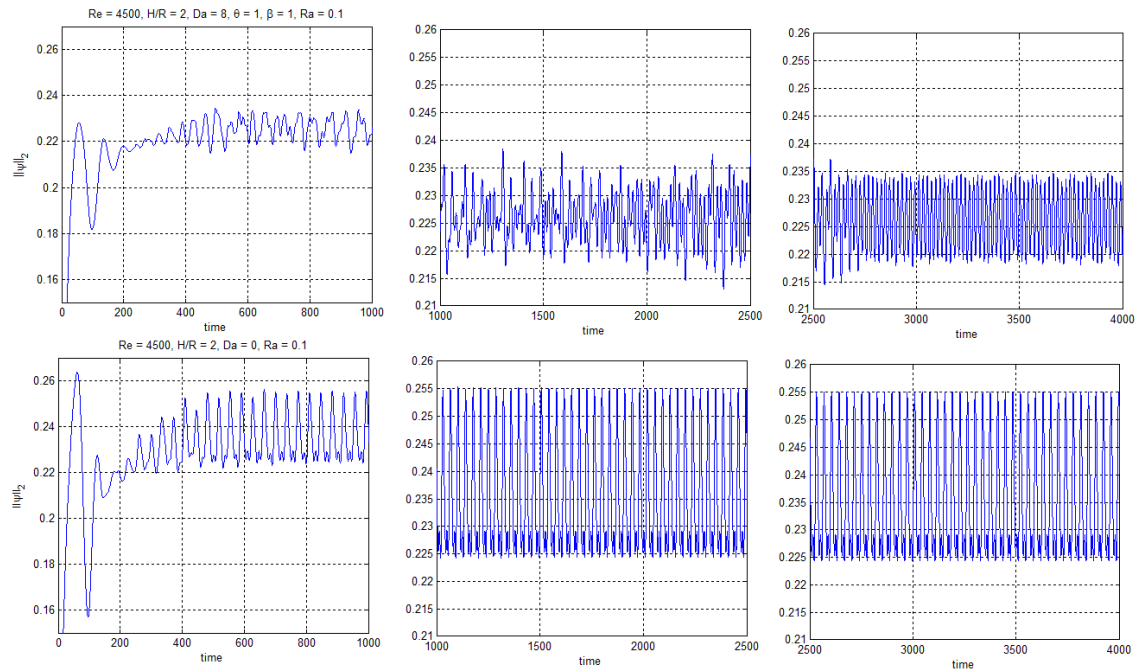


Figure 24: $H/R = 2$, $Re = 4500$, $Ec = 0$, $Pr = 0.7$, $Ra = 0.1$, with thermal bath B.C. for T , showing $\|\psi\|_2$ for $Da = 8$, $\beta = 1$, $\theta = 1$ (top) and (bottom) $Da = 0$.

References

- [1] J. Bebernes and D. Eberly. *Mathematical Problems from Combustion Theory*. App. Math. Sci. 83, Springer-Verlag (1989)
- [2] H. Caglar, N. Caglar, M. Ozer, A. Valaristos, A.N. Miliou, and A.N. Anagnostopoulos. Dynamics of the solution of Bratu's equation. *Nonlinear Analysis* 71, p. e672-e678 (2009)
- [3] L. Dupaigne. *Stable Solutions of Elliptic Partial Differential Equations*. CRC Press: Taylor & Francis Group (2011)
- [4] K.E. Gustafson and B.E. Eaton. Exact Solutions and Ignition parameters in the Arrhenius conduction theory of gaseous thermal explosion. *J. Applied Mathematics and Physics (ZAMP)*, Vol. 33 (1982)
- [5] A. Arakawa. Computational design for long-term numerical integration of the equations of fluid motion: two-dimensional incompressible flow. Part 1. *Journal of Computation Physics*, 135, 103-114, 1997. (Reprinted from Academic Press, 1966)
- [6] J. Beer and N. Syred. Combustion in Swirling Flows: A Review. *Combustion and Flame*, 23:143-201, 1974.
- [7] J. Choi, Z. Rusak and A. Kapila. Numerical Simulation of Premixed Chemical Reactions with Swirl. *Combustion Theory and Modelling*, 6.11:863-887, 2007.
- [8] G. Continillo, V. Faraoni, P.L. Maffettone and S. Crescitelli. Non-linear dynamics of a self-igniting reaction diffusion system. *Chemical Engineering Science*, 55:303-309, 2000.
- [9] M.P. Escudier. Observations of the flow produced in a cylindrical container by a rotating endwall. *Experiments in Fluids*, 2, 189-196, 1984.
- [10] M. P. Escudier, J. O'Leary, and R. J. Poole. Flow produced in a conical container by a rotating endwall. *Int. J. Heat Fluid Flow* 28, 1418-1428 (2007).
- [11] H. Gomez, J. Paris. Numerical simulations of Asymptotic states of the damped Kuramoto-Sivashinsky equation. *Phys. Rev. E, Volume 83, Issue 4* 2011
- [12] M. Hafez and J. Ahmad. Vortex Breakdown Simulation, Part-III: Compressibility Effects. *Fourth Symposium on Numerical and Physical Aspects of Aerodynamic Flows Jan. 16-19, 1989*.
- [13] M. Hafez, G. Kuruwila, and M.D. Salas. *Numerical Study of Vortex Breakdown*. Applied Numerical Mathematics 2, p. 291-302 (1986)
- [14] V. N. Shtern, M.M. Torregrosa, and M. A. Herrada. Effect of swirl decay on vortex breakdown in a confined steady axisymmetric flow. *Phys. Fluids* 24, 043601 (2012)

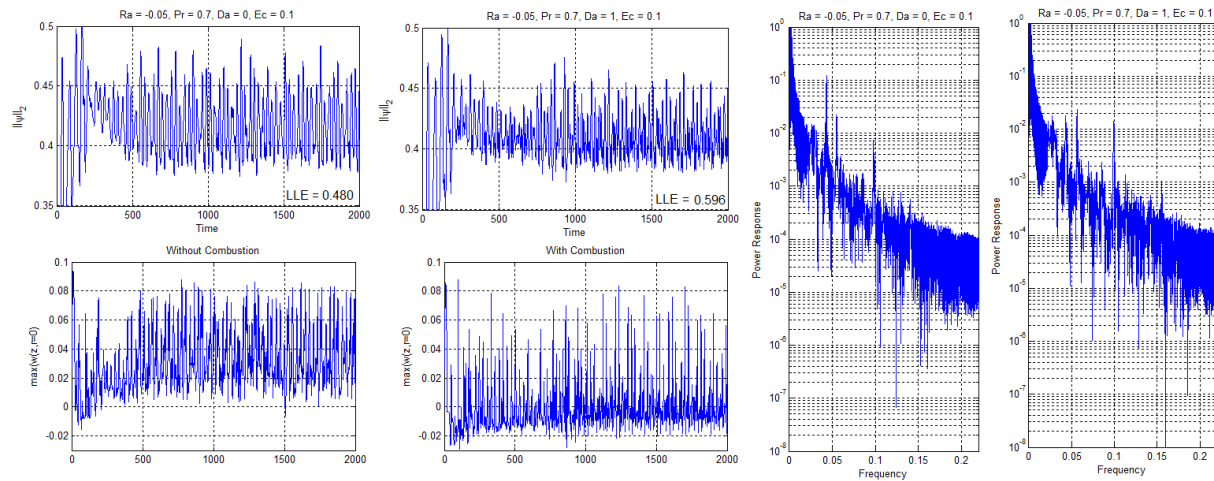


Figure 25: $H/R = 2$, $Re = 4500$, with heated wall B.C. for T , showing signal density for $\|\psi\|_2$ (top) and $\|w(x, r = 0)\|_\infty$ (bottom) as well as the power spectrum of $\|\psi\|_2$ time series (far right) with combustion (right) $Pr = 0.7$, $Ra = -0.05$, $Da = 1$, $\Theta = 1$, $\beta = 1$, $Ec = 0.1$, and without (left) $Da = 0$.

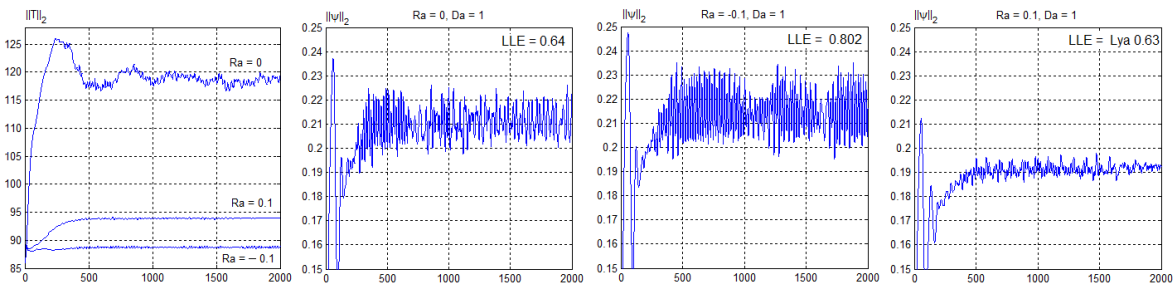


Figure 26: $H/R = 2$, $Re = 6000$, $Ec = 0$, $Pr = 0.7$, $Da = 1$, $\Theta = 3$, $\beta = 4$, and thermal bath B.C. for T . $\|T\|_2$ for $Ra = [-0.1, 0, 0.1]$ (left) and $\|\psi\|_2$ time series for $Ra = 0$ (Left middle) $Ra = -0.1$ (right middle) $Ra = 0.1$ (right).

- [15] Y. Huang and V. Yang. Dynamics and stability of lean-premixed swirl-stabilized combustion. *Progress in Energy and Combustion Science*, 35:293-364, 2009.
- [16] Gray, B.F; Scott, S. K. *The Influence of Initial Temperature-Excess on Critical Conditions for Thermal Explosion*. Combustion and Flame 61, p. 227-236 (1985)
- [17] K.K. Kuo, *Principles of Combustion*. John Wiley & Sons, Inc. (1986)
- [18] H.J. Lugt and M. Abboud. *Axisymmetric vortex breakdown with and without temperature effects in a container with a rotating lid*. J. Fluid Mech. 179, 179-200, (1987)
- [19] H. K. Moffat. Viscous and resistive eddies near a sharp corner. *J. Fluid Mech.* 18, 1-18 (1964)
- [20] D.C. Jespersen. Arakawa's method is a finite-element method. *Journal of Computation Physics*, 16, 383-390, 1974.
- [21] J.M. Lopez. Axisymmetric vortex breakdown Part 1. Confined swirling flow. *J. Fluid Mech.* vol. 221, p. 533-552, 1990.
- [22] L.C. Felgueroso and J. Peraire. A time-adaptive finite volume method for the Cahn-Hilliard and Kuramoto-Sivashinsky equations. *Journal Computational Physics* 227, 9985-10017, 2008.
- [23] A. Bayliss and B.J. Matkowsky. Bifurcation, pattern formation and chaos in combustion. ref: P.C. Fife, A. Linan and F. Williams. *Dynamical Issues in Combustion Theory*. Springer-Verlag New York. 1991.
- [24] B. Rogg. *The effect of Lewis number greater than unity on an unsteady propagating flame with one-step chemistry*. in N. Peters and J. Warnatz. *Numerical Methods in Laminar Flame Propagation A GAMM-Workshop*, Friedr. Vieweg & Son (1982)

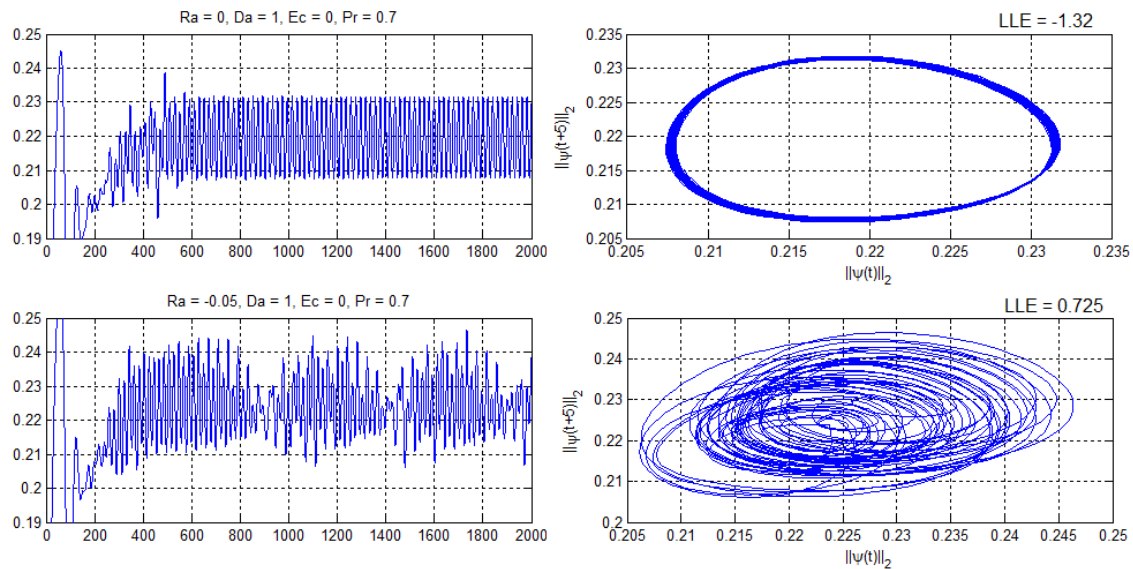


Figure 27: $H/R = 2$, $Re = 5500$, and thermal bath B.C. for T with $Ra = 0$, $LLE \approx -1.32$ (top) and $Ra = -0.05$, $LLE \approx 0.752$ (bottom), showing transition in $\|\psi\|_2$ to aperiodicity due to combustion.

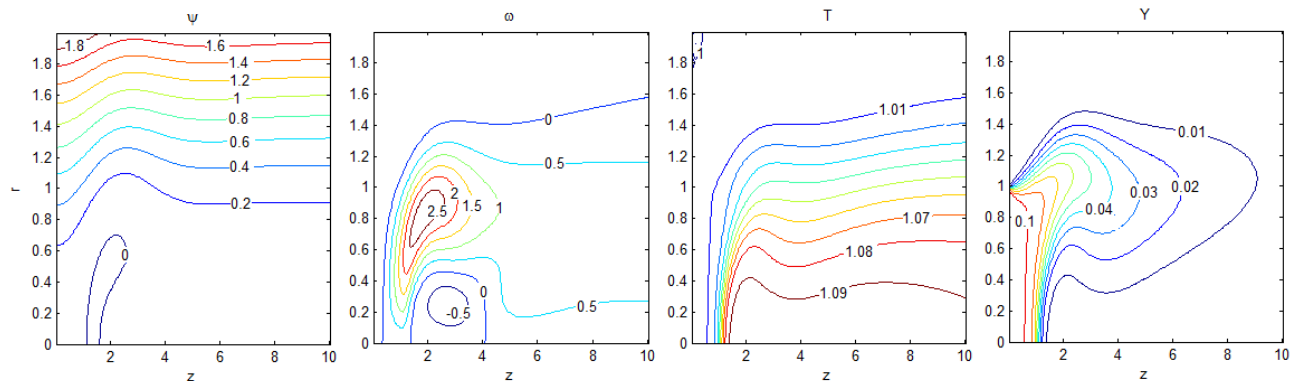


Figure 28: ψ , ω , Y , T for a steady compressible flow with premixed combustion (left) and without (right).

- [25] S.J. Ruuth. Implicit-explicit methods for reaction-diffusion problems in pattern formation. *J. Math. Biol.* 34:148-176, 1995.
- [26] E.A. Shabana. Numerical simulation of unsteady axisymmetric vortex breakdown including heat transfer. *Ph.D Thesis. University of California, Davis*, 1994.
- [27] A.K. Kassam. L.N. Trefethen. *Fourth Order Time Stepping for Stiff PDES* SIAM J. Scientific Computing 26(4): 1214-1233 (2005)
- [28] F. Sotiropoulos and Y. Ventikos and T. C. Lackey. Chaotic advection in three-dimensional stationary vortex-breakdown bubbles: Sil'nikov's chaos and the devil's staircase. *J. Fluid Mech.* vol. 444, 257-297. 2001.
- [29] J. C. Sprott, *Chaos and Time-Series Analysis* (Oxford University Press, 2003), pp.116-117.
- [30] Y. Zeldovich; G. Barenblatt; V.B. Librovich; G.M. Makhviladze. *The Mathematical Theory of Combustion and Explosions*. Consultants Bureau (1985)

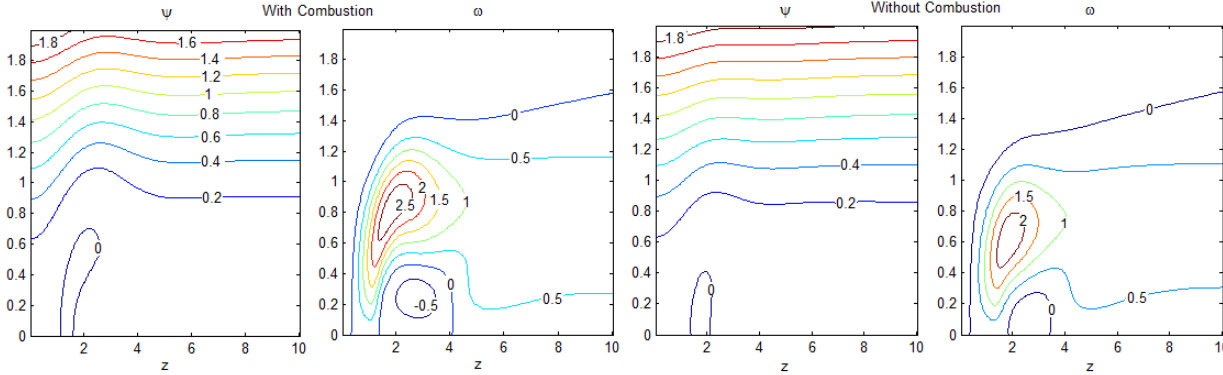


Figure 29: ψ, ω, Y, T for a steady compressible flow with small heat release.